New Instruments and Experimental Methods

PHYSICAL MEASUREMENTS ON PHOTOGRAPHS OF PARTICLE TRACKS IN BUBBLE CHAMBERS

I. I. PERSHIN

Usp. Fiz. Nauk **73**, 559-581 (March, 1961)

1. CHARACTERISTIC FEATURES OF BUBBLE CHAMBERS

1.1. Introduction

BUBBLE chambers are playing an increasingly important role in experiments with high-energy particles.

Measurements carried out on the photographs of particle tracks in bubble chambers are based on methods developed in connection with cloud chambers and photographic emulsions, but nevertheless differ from these methods in some ways. This difference in the methods is due to different optical conditions, to the specific track structure in the bubble chamber, and also to a different relation between the measured quantities and the background.

In the study of high-energy particles produced by an accelerator, information of a statistical nature which is required in the majority of cases is collected through a detailed analysis of a large number of interactions of interest. Methods involving electronic detecting devices have therefore been developed extensively for such investigations. However, by studying complex processes in bubble chambers, we can collect a great amount of information during a period of time that is comparable with that necessary for the development of special electronic detectors. Bubble chambers are more efficient than other track detectors. Their advantages are especially felt in the study and search of rare events. This is demonstrated in Table I, which is based on material from the review of Glaser.[23]

The high efficiency of bubble chambers for the detection of events involving fast particles is mainly due to three factors: a) the density of matter in bubble chambers is greater than the gas density in the usual cloud chambers by a factor of approximately 10^3, 2) bubble chambers operate with a cycle of several

Table I. Comparative characteristics of bubble chambers and emulsions used for the detection of nuclear particle tracks, for a track length of 50 cm

Detector	Density of working liquid ρ, g/cm^2	Radiation length λ, cm	Stopping power for 50-cm chamber length, g/cm^2	Efficiency*	
				Events per day for $\sigma_{nucleon} = 10^{-30}$ cm^2 = 1 mb	Events per picture for $\sigma_{nucleon} = 10^{-27}$ cm^2 = 1 mb
Argon cloud chamber at 1 atm	0.0017	11600	0.085	0.015	0.0003
Hydrogen diffusion chamber at 20 atm	0.0019	36300	0.095	0.016	0.0003
Hydrogen bubble chamber	0.05	1380	2.5	0.43	0.008
Helium bubble chamber	0.10	963	5.0	0.86	0.015
Propane bubble chamber	0.43	110	22	3.7	0.07
Bubble chamber with $SnCl_4$	1.5	7.35	75	13	0.23
Xenon bubble chamber	2.3	3.1	115	20	0.34
Nuclear emulsions (AgBr)	4.0	2.8	200	34	0.59

*It is assumed that 50 particles traverse the chamber every 5 sec.

Table II. Working characteristics of liquids used in bubble chambers

Liquid	Θ_{boil} °C	Θ_{crit} °C	Θ_{work} experimental	P_{crit} atm	$P_{\infty\ work}$ atm	d_{work} g/cm³	Radiation length	Bibliography
Hydrogen-containing liquids and helium								
Hydrogen, H_2*	−253.8	−240	27° K	12.8	5	0.06		3, 4, 5, 6, 10, 18
Propane, C_3H_8	− 42.2	95.6	64° C	43	24	0.42		7, 8, 9, 17
Ethylene, C_2H_4	−103.9	9.7	−20° C	50.9	26	0.41		11
Helium, He	−268.9	−267.9	4.2° K	2.26	1	0.12		12
Liquids with high atomic number								
Xenon, Xe	−107.1	16.6	−20° C	58.2	26.7	2.3	3.1 cm	11, 16
$SnCl_4$ 65% / $CClF_3$ 35%			20° C		28.5	1.7	9.1 "	13
Some heavy liquids, and mixtures with suitable thermodynamic properties								
Freon 13	−80	28.8	0° C	39.4	20		33 g/cm²	24, 25
Freon 12	−29.8	111.5	75° C	40.8	20		25 g/cm²	24, 25
C_2F_6/C_3F_8 (K=0.44**)			21° C		14	1.28	27 cm	31
C_3F_8			37.9° C		13.4	1.25	28.4 "	31
SF_6			15.1° C		18.7	1.42	20.5 "	31
SF_6/C_2ClF_5 (K=3.35)			17.9° C		16.6	1.36	21.5 "	31
SF_6/C_2ClF_5 (K=0.87)			24.5° C		15.5	1.30	22.8 "	31
SF_6/C_2ClF_5 (K=0.36)			30.9° C		14.6	1.25	23.8 "	31

*Hydrogen chamber may be filled with deuterium.[10]
**K = ratio of the first component to the second (according to weight).

seconds, and 3) modern bubble chambers possess considerable geometric dimensions. The large volume available for the detection of interesting events facilitates both the search for interactions and the study of correlation between events. In connection with this, favorable conditions arise for the automatization of the track analysis.

In order to obtain consistent results, certain conditions, which ensure the stability of the chamber operation, should be observed.

The present review is devoted to a discussion of the measurements of those physical quantities necessary for particle identification in bubble-chamber photographs, and also to problems involving the choice of the bubble-chamber operating conditions.

1.2. Working Liquids Used in Bubble Chambers

In 1952, Glaser[1] discovered that a superheated liquid boils upon the passage of ionizing radiation. The use of liquid (bubble) chambers for the detection of high-energy particles began in 1953 — 1954, after Glaser had established[2] that ionizing particles, passing through a volume filled with superheated liquid, leave tracks consisting of bubbles. During the following years, bubble chambers were successfully used in work with accelerators, intensive investigations were made of the operating characteristics of different liquids and of the operating conditions of chambers, and a method was developed for making measurements on particle-track photographs. The operating characteristics of liquids presently used in bubble chambers are given in Table II.

In addition to those liquids mentioned in Table II, others are known which are sensitive to radiation in the superheated state. Many of these liquids possess properties that can be used advantageously in various physical investigations, but they are not convenient to work with because of high working pressures and temperatures, or because they are toxic or of insufficient chemical stability. Among these are, for example, $SnCl_4$, WF_6, and TeF_6.[26] In principle, these liquids can be used instead of the expensive xenon to fill large bubble chambers, and in investigations for which a short radiation length of the target matter is necessary. A high neutron-detection efficiency can be attained with BCl_3.[24] In many investigations and reviews,[3-20] the properties of a great number of liquids, liquid mixtures, and gasified liquids used in bubble-chambers are discussed.

For every specific case, the choice of the working liquid for the bubble chamber is determined by its suitability as a target for the given physical problem, and by considerations of convenience in use. Particle production and decay are presently the main subjects of investigation with high-energy particle accelerators. For the study of particle production, the results obtained in hydrogen chambers are the most interesting, since they have the advantage of a pure proton target. For the study of decay phenomena, the composition of

Table III. Range-energy relation for bubble chambers (range in the substance filling the chamber, cm)

Energy, Mev	Liquid-hydrogen chamber T = 27.6 ± 0.1°K, hydrogen density ρ = (5.86 ± 0.06) × 10^{-2} g/cm³				Propane chamber (technical propane) ρ = 0.42 g/cm³		Freon chamber (50% mixture freon 12 – freon 13) ρ = 1.14 g/cm³	
	μ meson	π meson	K meson	proton	π meson	proton	π meson	proton
5	1,5	1.2	0.43	0,25	0.33		0,18	
10	5,5	4,4	1.5	0,95	1.2	0,25	0.6	0.15
50	90	75	28	17	20	4,6	10,3	2.5
100	260	230	100	62	58	17	30,5	8.8
500	1800	1800	1350	980	460	250	240	130
1000	3800	3800	3300	2700	1000	690	—	350

the working liquid is not critical, and it is best to use large chambers filled with the substance most convenient for the work. Chambers filled with high-Z substances possess known advantages for these investigations. These advantages are due both to the high efficiency of the high-energy γ-ray detection and to the greater possibility of using multiple-scattering measurements for particle identification. Dual chamber fillings have also been proposed* thus, one part of the chamber would constitute a hydrogen-containing target, while the other would be suited for observing decay phenomena and would be filled with a high-Z substance.

In studying the interaction of high-energy particles with a given nucleus, the composition of the liquid naturally depends on the requirements of the physical problem. For this type of investigation, chambers filled with hydrogen, deuterium, and helium are of special interest. However, in a number of cases, simpler chambers filled with compounds that include these nuclei (e.g., propane, deuteropropane, etc.) can be used instead. The choice of the working liquid is not very critical in many investigations of particle polarization.

1.3. Range of Particles in Bubble Chambers

The ranges of particles in those liquids most frequently used in bubble chambers are given in Table III.

The ranges for liquid hydrogen and propane are determined from energy-range relations,[32] taking into account the range of the μ meson originating in the π-μ-e decay of stopping π mesons, which has been determined in experiments. Data for the liquid-hydrogen chamber are taken from graphs of Clark and Deal,[32] and those for freon from reference 25. The ranges in the xenon chamber are shorter than those in the propane chamber by a factor of approximately 2.8.

2. COORDINATE MEASUREMENTS IN BUBBLE CHAMBERS

2.1. Relation Between the Particle Track in a Bubble Chamber and its Photographic Image. Distortions in Bubble Chambers

The bubble string forming the observed track of the particle traversing the chamber represents only to a certain extent the real particle trajectory. The deviation between the visible track and the trajectory is, as a rule, small in properly-designed instruments, and in many cases may be neglected. However, in any particular case, it is necessary to estimate its effect on the measured quantities. Many factors influence the deviation. These factors can be divided into two categories: optical factors related to the nature of the bubble-image formation, and factors producing an apparent curvature (distortion) of the track.

Attention has been drawn to the considerable role played by optical factors.[33] After having considered the production mechanism of the glowing centers that make up the visible image of the bubble string, the authors of reference 33 have shown that these light centers are essentially not glowing bubbles, but the images of the light source produced by negative spherical lenses, i.e., by the bubbles in the liquid. According to a calculation[33] for paraxial rays coming from infinity, the distance f′ from the center of a spherical lens of radius R to the image is

$$f' = \frac{1}{2} R \frac{n_2}{\Delta n}, \qquad (1)$$

where Δn is the difference between the refractive index n_1 of the working liquid and the refractive index n_2 of the gas in the bubble. From Eq. (1) it follows that if Δn is small the difference between the bubble position and its image will be considerable. Thus, for liquid hydrogen, this difference amounts to 6R, where R is the bubble radius. In practice, the difference between the bubble position and the light center depends not only on Δn, but on the distance of the light source as well.

The factors leading to an apparent (false) curvature of the particle tracks can, in turn, be subdivided into random deflections and systematic distortions. Random deflections are due mainly to multiple scattering of the particles passing through the chamber and to errors in the measurement of the coordinates.

Systematic distortions are due a) to the presence in the liquid of convection currents caused by heat transfer and by the general motion of the liquid during expansion, b) to the presence in the liquid of turbulence leading to local distortion, and c) to defects in the optical system used in the photography.

The apparent track curvature due to the multiple scattering can be estimated from theoretical consid-

*See, e.g., the remark of Budde to paper[28] presented at the Accelerator Conference in Geneva, 1959.

erations. The average curvature ρ of the track of a particle with momentum p and velocity βc traversing a medium with atomic number Z and density A nuclei/cm^3 is given by the equation[34]

$$\frac{1}{\varrho} = \left(\frac{16\pi}{3}\right)^{1/2} \frac{ZN^{1/2} r_e m_e c^2}{L^{1/2} p\beta c} B, \qquad (2)$$

where

$$r_e = 2.8 \cdot 10^{-13}\ \text{cm}, \quad m_e c^2 = 0.51\ \text{Mev},$$

$$B = \left[\ln\left(\frac{\theta_{max}}{\theta_{min}}\right)\right]^{1/2}, \quad \theta_{min} = \frac{mcZ^{1/3}}{137p}.$$

The exact determination of θ_{max} is difficult, but from Eq. (2) it is clear that its choice is not critical. (We can, for instance, set θ_{max} equal to one.)

The distortion due to convection currents and turbulence depends mainly on the chamber construction. Results of a study of these distortions for a number of hydrogen and propane chambers have recently been published. The results pertain to several chamber constructions, and are interesting from the point of view of the methods used for measuring the distortion. Using any of these methods, we can establish a general picture of the distribution of the distortions, and apply a correction to the measured coordinates according to the results obtained.

If the chamber is designed properly, and the track photographed at the optimum moment, the systematic distortions are not large in most regions of even small bubble chambers. Thus, it has been found[35] that, for a hydrogen chamber 10 cm in diameter and 6 cm high with vertical windows and piston compression, convection currents arising in the thermostated system do not cause an appreciable systematic distortion. On the other hand, in a hydrogen chamber 25 cm in diameter with horizontal windows and gas compression, considerable local distortion was observed along the axis passing through the expansion system.[36] In a large propane chamber,[37] considerable systematic distortion was observed which, by itself, (i.e., not taking the multiple scattering into account) was approximately one order of magnitude greater than the systematic distortion in the best-constructed cloud chambers.

2.2. Stereoscopy of Bubble Chambers

In order to determine the position of the particle tracks in bubble chambers, the tracks are photographed using, in the simplest case, a two-lens stereoscopic camera with identical lenses having parallel optical axes. The film plane is usually parallel to the median plane of the bubble chamber.

Stereoscopic relations between the particle tracks in the bubble chamber and their images on the film are different from the relations for usual cloud and diffusion chambers, because of the thick glass windows of the bubble chamber and because of the refractive index of the working liquid in the chamber.

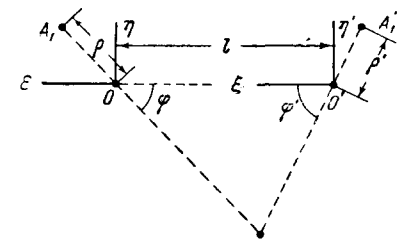

FIG. 1. Coordinate system in the film plane. The plane of the drawing coincides with the film plane.

The reconstruction of the three-dimensional picture can be achieved by projecting the obtained track photographs on a screen, using a stereo projector which is optically identical to the camera used. To remove the secondary optical effects in projection it is necessary to use instruments that compensate for the glass windows of the chamber and of the thermostatic bath, and also for the layer of the working liquid in the bubble chamber. However, this would require the construction of special stereo projectors, and would not be convenient for work with instruments for the automatic evaluation of particle tracks.

A more economical method is to calculate the actual coordinates from the coordinates measured in the plane of the film or on projections of the film on a screen.

The relation between the coordinates measured on the plane and the actual coordinates can, within the limitations of geometrical optics, be found using the simplest geometric calculations.[38]

Let O and O′ (Fig. 1) correspond to the points of intersection of the optical axes of the camera lenses with the film plane, A and A′ —the images on the film of a point a within the bubble chamber, and (ρ, φ) and (ρ', φ') —the polar coordinates of the points A and A′ on the film. Furthermore (see Fig. 2), let f be the focal length of the lenses, d the distance from the center of the lens to the front window of the chamber, δ the thickness of the glass, z the depth of the point in the chamber, n the refractive index of the liquid in the chamber, n* the refractive index of the front window of the chamber, and l the distance between the optical axes of the camera lenses. Then, the spatial Cartesian coordinates (x, y, z) of the point a are given in terms of the coordinates (ρ, φ) and (ρ', φ') on the film by the expressions:[38]

$$x = \frac{l \sin\varphi' \cos\varphi}{\sin(\varphi + \varphi')}, \qquad (3)$$

$$y = \frac{l \sin\varphi' \sin\varphi}{\sin(\varphi + \varphi')}, \qquad (4)$$

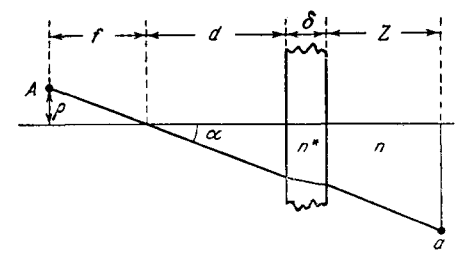

FIG. 2. Notation for the ray path in the photography of bubble chambers.

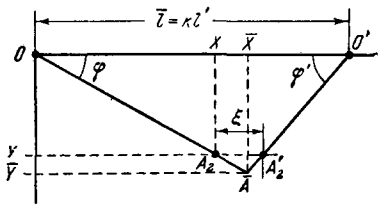

FIG. 3. Coordinate system in the screen plane on which the image of the track particles is projected. Plane of the drawing coincides with the screen plane.

$$z=\left\{\frac{l\sin\varphi'}{\varrho\sin(\varphi+\varphi')}-\frac{d}{f}-\delta\left[n^{*2}f^2+(n^{*2}-1)\varrho^2\right]^{-1/2}\right\}\{n^2f^2+(n^2-1)\varrho^2\}^{1/2}. \quad (5)$$

These formulas become considerably simpler if the photographs are taken from a distance at which the subtending angle of the cone of rays can be assumed to be small (i.e., where $\tan\alpha\approx\sin\alpha\approx\alpha$). Such conditions are always satisfied for the central part of the chamber. We then have

$$x=\frac{l\xi}{\xi-\xi'}, \quad (6)$$

$$y=\frac{l\eta}{\eta-\eta'}, \quad (7)$$

$$z\simeq n\left(\frac{lf}{\xi-\xi'}-d-\frac{\delta}{n^*}\right). \quad (8)$$

where ξ, ξ', η, and η' are the Cartesian coordinates of points A and A' measured directly on the film.

In calculating the time coordinates of points in the chamber from the coordinates of the points measured on the screen projection of the film, we obtain the following approximate relations:[38]

$$x=\frac{\bar{X}}{k}=\frac{Xl}{kl-\zeta}, \quad (9)$$

$$y=\frac{\bar{Y}}{k}=\frac{Yl}{kl-\zeta}, \quad (10)$$

$$z\simeq n\left(f\frac{jl}{kl-\zeta}-d-\frac{\delta}{n^*}\right). \quad (11)$$

where j is the magnification of projection, and k is the factor correcting for the change of the projection base (the distance between the optical axes of the lenses). The remaining symbols are either similar to those of equations (3) to (8), or are directly clear from Fig. 3. (In Fig. 3, points A_2 and A_2' correspond to the projections of the images of points A_1 and A_1' on the film, while O and O' correspond to the points of intersection of the optical axes of the projector lenses with the screen plane.)

The above relations correspond to the most-frequently used method of photographing the particle tracks using a two-lens stereoscopic camera. Such a method is, however, insufficient to ensure uniformly accurate results for various orientations of the photographed plane (such as strongly inclined tracks, or tracks parallel to the stereoscopic base). To increase the accuracy it is necessary to use at least three non-collinear lenses. In reference 39 is described a convenient approximate method for the graphical analysis of particle-track photographs in bubble chambers, useful in work with a three-lens stereoscopic camera.

Usually, to simplify the calculation of the influence of the refractive index of the liquid in the bubble chamber, fiducial marks are placed on the chamber window, and these are photographed together with the particle tracks. Equations (3) to (11) can easily be transformed so that, in the calculations, one can take the photographs of the marks as the origin of the coordinates.

2.3. Projective Methods of Particle-Track Analysis

In those cases where the investigated physical process possesses an axial symmetry, it is often possible to study the event projected on a plane, instead of applying the full three-dimensional analysis. To do this, it is, first of all, necessary to transform the three-dimensional relations to the equivalent projected relations. The relations between the events are then studied either directly from the film, or after projecting the film on a screen by means of a simple projector.

Such a method has been used successfully by a number of investigators[40-42] for the study of asymmetry in the π-μ-e decay of mesons stopping in the chamber, in a check on the hypothesis of parity non-conservation in weak interactions. This method can have wide application in the study of problems involving the polarization phenomena in nuclear interactions of high-energy particles.

3. MEASUREMENT OF PARTICLE VELOCITY

3.1. Conditions Necessary for the Measurement of Particle Velocity in Bubble Chambers

The problem of measuring the velocity of particles from the photographs of their bubble-chamber tracks has attracted the attention of investigators from the very beginning of the development of the bubble-chamber method. In the first papers describing the action of bubble chambers (e.g., reference 7), differences in the track densities for particles having various velocities were mentioned. Since no exact theory of the bubble-chamber operation exists, it is at present

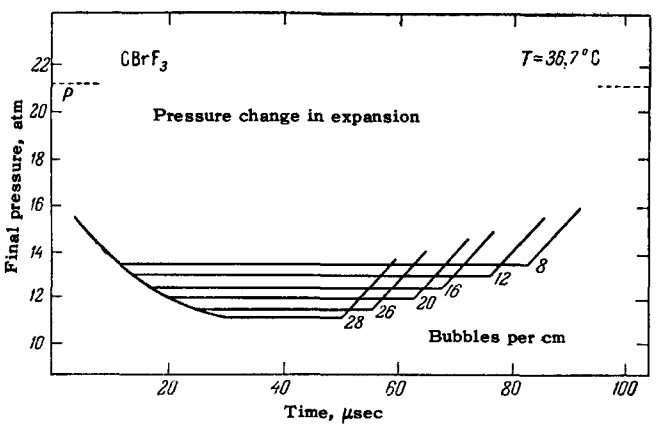

FIG. 4. Number of bubbles per cm of a 30-Mev electron track as a function of the final pressure. The bubble chamber was filled with $CBrF_3$ at 36.7°C.

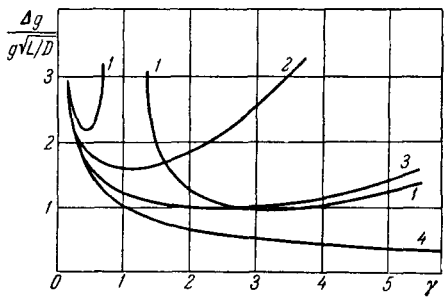

FIG. 5. The error $\Delta g/g\sqrt{\frac{L}{D}}$ as a function of $\gamma = gD'$ for various methods of accounting for the overlap of bubble images. 1 – gap-density method, 2 – mean gap-length method, 3 – measurement of the track porosity, 4 – measurement accuracy for an absence of overlap.

not possible to write a relation between the particle velocity and the bubble density along the track. Attempts in this direction (see, e.g., references 43 and 44), are to a great extent arbitrary. The relation between the particle velocity and the number of bubbles per cm of track length ("bubble density along the track") is at present determined experimentally. In finding this relation, it is necessary to preserve certain conditions with respect to the construction and the method of operation of the chamber, as well as with respect to the evaluation of the particle tracks. This is due to a number of reasons.

1. The bubble density of a particle track varies greatly with pressure and with the degree of overheating of the liquid.* In Fig. 4, experimental graphs from reference 45 are presented, showing the variation of the bubble density with the final chamber pressure. It was found[48] that, with the temperature of propane varying from 55 to 59° C, the bubble density varied from 20 to 55 bubbles per cm (see Fig. 7).

In view of the above, exact measurements of the particle velocity are possible only in bubble chambers with controlled final pressure and temperature. It was found[45] that, in order to obtain a 5% accuracy in the number of bubbles in a chamber filled with $CBrF_3$, it is necessary to control the temperature to within ± 0.1° C, and the final pressure to within 0.05 atm.

2. The bubble density as observed directly on photographs is, in general, different from the actual density produced in the chamber during the passage of particles because of the overlapping of bubble images, and because of the coalescence of closely lying bubbles. For dense tracks, the difference between the true number of bubbles and that observed on photographs may be very considerable, and may amount to several times. Therefore, in determining the real bubble density, a correction for the overlapping of bubble images should be introduced.

*The superheat of the liquid in the chamber is defined as the difference $p_\infty - P$, where p_∞ is the saturated-vapor pressure at the working temperature, and P is the pressure acting on the liquid at the final moment of pressure reduction.

3. Only tracks consisting of small bubbles are found to be useful for particle velocity measurements. Only for small bubbles is the bubble distribution, corresponding to the random nature of the ionization process, not distorted by interference phenomena between the bubbles.

The stability of the final pressure depends on the chamber construction. In the majority of existing bubble-chamber designs, control of the final pressure is not provided, and the final pressure is determined by a number of varying factors, such as velocity of expansion, pressure of the vapor originating in the ebullition of the liquid and acting on the structure of the chamber, heat-exchange conditions, etc. A prototype of a chamber incorporating a special system to control the final pressure is described in reference 9. The contribution of all the factors which determine the operation of a chamber with a controlled final pressure has been studied in detail in reference 45.

3.2. Correction for the Overlapping of Bubble Images

An analysis of the presently used methods of applying a correction for the overlapping of bubble images, taking the specific structure of the particle tracks in bubble chambers into account, is given in reference 46.

Let g be the mean density of bubble images, D the diameter of the bubble image, l the gap length, and l_0 the minimum gap length taken into account in the measurements (gaps with a length less than D/2 must be disregarded; see reference 9). Furthermore, let $\gamma = gD$, L be the total track length, and $D' = D + l_0$. Then, if the track of a particle consists of sufficiently small bubbles, the gaps (their length and number) have a Poisson distribution[9] and g can be determined by counting the gaps, either from the mean gap length or by determining the "porosity" of the track (the mean ratio of the total length of all gaps longer than l_0 to the total track length).

Each of the above-mentioned methods has a different statistical accuracy and range of application (see Fig. 5, taken from reference 46). We shall list here the main considerations applying to these methods, according to reference 46.

For tracks that are not very dense ($gD' < 2.9$), the best accuracy is attained by the method of measuring the track porosity. The mean track porosity is given by

$$v = \exp(-\gamma). \tag{12}$$

The relative error in measuring the value g is, in that case,

$$\left(\frac{\Delta g}{g}\right)_v = \sqrt{\frac{D'}{L}}\sqrt{2}\,\gamma^{-3/2}(\exp\gamma - \gamma - 1)^{1/2}. \tag{13}$$

For the same range of values of gD', the method of mean gap length is also applicable, although it produces a somewhat lower accuracy. If λ is the mean gap length minus l_0, then

$$\lambda = \frac{1}{g} \tag{14}$$

and

$$\left(\frac{\Delta g}{g}\right)_\lambda = \sqrt{\frac{D'}{L}}\left(\frac{\exp\gamma}{\gamma}\right)^{1/2}. \tag{15}$$

For dense tracks ($gD' > 2.9$), the best method is the method of measuring the mean number of gaps longer than l_0. If n is the mean density of gaps longer than l_0, then

$$n = g\exp(-\gamma), \tag{16}$$

$$\left(\frac{\Delta g}{g}\right)_n = \sqrt{\frac{D'}{L}}\left(\frac{\exp\gamma}{\gamma} - 2\right)^{1/2} |1-\gamma|^{-1}. \tag{17}$$

In practice, measurements according to the method of the mean gap length have become widespread for very dense tracks, while the method of counting the number of gaps is frequently used for particle tracks with a high bubble density.

3.3. Experimental Relation Between the Bubble Density along the Track of a Particle and its Velocity. Determination of Particle Momentum from the Measured Bubble Density

We shall now review the results of measuring the bubble density as a function of particle velocity in bubble chambers filled with different liquids.

From measurements of g in a propane bubble chamber (without control of the final pressure), the following relation[47] was found by a direct bubble count:

$$g = \frac{A}{\beta^2} + B(T), \tag{18}$$

where $A = 9.2 \pm 0.2$ cm^{-1} for the temperature range of 55 to 59.5° C, and where B(T) is a certain function of the temperature.

In this experiment the bubble density varied over the series of photographs taken, and the number of bubbles counted along the investigated track was normalized with respect to the bubble density along the tracks of particles with minimum ionization which were included in each photograph.

By carrying out such measurements in a propane chamber with controlled final pressure and temperature (temperature kept constant to within ±0.1° C), and taking the correction for overlap into account, it was found[9] that

$$g = \frac{A'(T)}{\beta^2} \tag{19}$$

for a wide range of particle velocities (Fig. 6). Moreover, the measurements of g were absolute: in determining the bubble density along the track of any particle, it was not necessary to normalize the result with respect to the bubble density in minimum-ionization particle tracks. The same method applied to the determination of g in a chamber filled with $CBrF_3$ has produced the same result.[45]

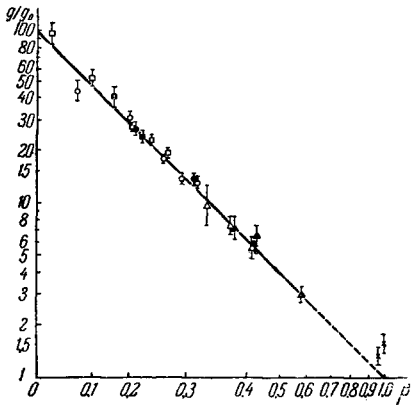

FIG. 6. Variation of g/g_0 with β for a propane bubble chamber. Both axes are logarithmic. The chamber is operated with constant final pressure under various operating conditions. Notation: For conditions No. 1: ○ – protons, □ – deuterons, and △ – π mesons. For conditions No. 2: ● – protons, ■ – deuterons, and × – electrons. For conditions No. 3: ▲ – π mesons and × – electrons.

In the operation of a bubble chamber with controlled final pressure, the bubble density is constant for tracks of different particles having the same velocity, and it is easily possible to vary the bubble density of the particle tracks by changing the operating conditions of the chamber. From the curves shown in Fig. 4, it can be seen that, by varying the value of the final pressure and keeping the working temperature constant, we can vary the bubble density of the particle tracks by a factor of several times. Using such a method, the authors of reference 9 were able to measure the bubble density of tracks of particles having a specific ionization several ten times greater than minimum ionization.

In reference 48, the relative measurements of g were repeated for the same particle tracks which were measured in reference 47, but, in reducing the results of the measurements, corrections were applied for the overlapping of bubble images. The true number

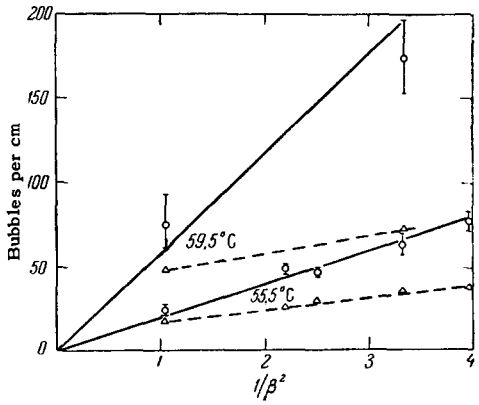

FIG. 7. Number of bubbles per cm as a function of $1/\beta^2$ for propane. The measurements were carried out on the same particle tracks by two different groups of investigators. The circles correspond to the results obtained in reference 48, and the triangles to those obtained in reference 47.

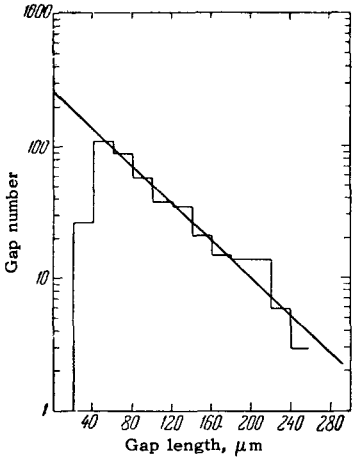

FIG. 8. Distribution of the number of gaps between bubbles as a function of the gap length measured on the film for a track with ionization equal to 2.3 minimum ionization (from measurements in a propane chamber at 55.5°C[48]).

of bubbles determined after introducing the correction for the overlapping was found to be considerably greater than that found by a direct bubble count (Fig. 7), and the dependence of g on β^2 was well described by Eq. (19), just as in references 9 and 45. It was also found that the gap-length distribution is, in that case, given by

$$f(l)=ge^{-gl}, \tag{20}$$

where g (the mean number of bubbles per unit track length) can be determined from the slope of the straight line drawn through experimental points, if the variation of the gap number with gap length is represented graphically using a logarithmic scale along the ordinate (Fig. 8).

An attempt to determine the variation of bubble density with β^2 was also made for a liquid-hydrogen chamber.[49] Because of the high bubble density of the particle track, the authors were able to measure directly the number of visible tracks of δ electrons along the particle tracks as a function of β^2. A single-valued relation between these variables has been found, and curves have been constructed which enable us to find the momentum or velocity of a particle as a function of the number of δ electrons observed along the particle track.

Thus, we can accept the claim that, under the conditions stated in Secs. 1 to 3 of the present chapter, an absolute measurement of the particle velocity in bubble chambers is possible. In all cases, it was found that the true bubble density along particle tracks is expressed by Eq. (19), within the limits of error of the measurements. Assuming that Eq. (19) is exact, we can find the momentum of particles with a known mass from the measured value of g. The error in the momentum determination is given by the equation

$$\frac{\Delta p}{p}=\left(\frac{\gamma^2}{2}\right)\frac{\Delta g}{g}, \tag{21}$$

where

$$\gamma^2=\frac{1}{1-\beta^2}.$$

Thus, for instance, if the velocity of a 400-Mev proton is measured by counting 100 bubbles, its momentum can be found with an accuracy of ±10% (taking only statistical errors into account).

The error to which the measurement of the variation of g with β^2 is subject at present does not as yet enable us to decide that the particle velocity enters this formula only in the quadratic term. It has been mentioned in this connection[48] that we cannot regard the results obtained as proof of the fact that the bubbles along particle tracks are produced at the end of the tracks of stopped δ electrons. The experimental data available are also consistent with another possibility: it is possible that the number of bubbles along particle tracks is proportional to the probable specific ionization (the mean value of the total ionization produced by the primary particle and by all secondary electrons having an energy greater than η). In such a case,

$$\left(\frac{dE}{dx}\right)_{Q<\eta}=\frac{2\pi N(Ze^2)^2}{mc^2\beta^2}\left[\ln\left(\frac{2mc^2\beta^2\eta}{(1-\beta^2)I^2}\right)-\beta^2\right], \tag{22}$$

where I is the mean ionization potential (equal to ~ 50 ev for propane). The quantity η for propane should be taken as ≥ 70 kev, and for this value the δ-electron track will be ≥ 200 μm and will be visible on particle-track photographs. After substituting the above values, we find that we should in such a case expect for propane

$$\left(\frac{dE}{dx}\right)_{Q<\eta}\simeq\frac{c}{\beta^{1.83}}. \tag{23}$$

Considering the existing experimental accuracy, this relation cannot be regarded as being different from a $1/\beta^2$ proportionality.

A further refinement of the variation of g with β^2 may follow from the explanation of the relativistic increase of the bubble density near $\beta = 1$. The relativistic increase of the bubble density has been observed by a number of authors,[9,23] but the results obtained are only qualitative because of the poor statistics.

4. MEASUREMENT OF PARTICLE MOMENTUM IN BUBBLE CHAMBERS OPERATING IN MAGNETIC FIELDS

A particle with velocity **v**, momentum **p**, and charge Ze moves in a magnetic field **H** along a helix wound on a cylinder of radius ρ.[50] The generating line of this cylinder is parallel to the magnetic field, and ρ is given by the equation

$$\frac{p\sin\theta}{Z}=300H\rho. \tag{24}$$

where the particle momentum is measured in ev/c, $H\rho$ is gauss-cm, and the charge in units of the electron charge. The accuracy of the momentum measurement is determined by the experimental error in

the measurement of ρ. The measured values of ρ differ from the true value because of instrumental errors and the multiple scattering.

The instrumental errors are equivalent to a diffusion of the particle tracks, and arise both in the process of production of the visible track in the chamber and in the photography. In the photographs of particle tracks in bubble chambers, the particle track is represented by very sharp round images of bubbles and, in measurements carried out on the film, the error in the determination of the bubble-image center is less than $1/10$ of the image diameter. (The diameter of a bubble-image on the film is ~ 20 μm.) If ρ is determined by measuring the sag s, then

$$\varrho = \frac{l^2}{8s}, \tag{25}$$

$$p = \frac{300 l^2 H}{8s}, \tag{26}$$

where l is the length of the trajectory corresponding to the measured sag s.

The instrumental errors lead to the error δs_A and, correspondingly, to the appearance of an apparent track curvature ρ_0 and an apparent momentum p_0, given by the equation

$$p_0 = \frac{300 l^2 H}{8 \delta s_A}. \tag{27}$$

The quantity p_0 is called the maximum detectable momentum.

Taking into account that $\delta p/p = \delta s/s$, we have

$$\left(\frac{\delta p}{p}\right)_A = \frac{p}{p_0}. \tag{28}$$

The mean value of δp_A is found from measurements of the track curvature of a very high-energy particle (for which the multiple scattering is negligible) without the magnetic field.

The relative error due to multiple scattering in measuring the particle momentum from a track length t is determined by the relation[51]

$$\frac{\Delta p}{p} \simeq \frac{\theta_s}{\omega t^{1/2}}, \tag{29}$$

where $\omega = 3 \times 10^{-4}$ (H/p). The mean angle of multiple scattering can be estimated from the formula[50]

$$\theta_s^2 = \frac{441}{\beta^2 p^2 x_0}, \tag{30}$$

where x_0 is the radiation length in cm for the given substance.

In hydrogen bubble chambers, the error due to scattering is relatively small, but in chambers filled with heavier liquids, the basic error in the determination of the particle momentum (using weak magnetic fields, see Sec. 5.3) is due to multiple scattering. Multiple scattering in these chambers may also lead to an error in determining the sign of the charge.

The probability of an error in the determination of the sign of the charge from a number of measurements on a group of homogeneous tracks, as deflected in a magnetic field, is given by the formula[52]

$$w = \left[1 + a \exp\left(-2\omega^2 \frac{t}{\theta_s^2}\right)\right]^{-1}, \tag{31}$$

where a is the ratio of the number of cases in which the charge was found negative to the number of cases in which it was found positive, for a given particle.

Table IV, taken from reference 8, shows the results of a calculation of the error in the determination of the sign in a propane bubble chamber at a magnetic-field intensity of 10 kilogauss. In order to obtain a 10% accuracy in the momentum measurement for a 5 cm track length of a relativistic particle, a magnetic field of ~ 7000 gauss is necessary for a hydrogen chamber, ~ 8200 gauss for a helium chamber, $\sim 25\,000$ gauss for a propane chamber, $\sim 94\,000$ gauss for a chamber filled with $PbCl_4$, and $\sim 140\,000$ gauss for a xenon chamber, according to the estimates of Glaser.[23] A field of 150 000 gauss would be necessary for a photographic emulsion.

5. MULTIPLE-SCATTERING MEASUREMENTS

5.1. Measurements Using the Constant-Cell Method

In bubble chambers filled with liquids heavier than hydrogen and helium, the multiple scattering of particles in the liquid is appreciable. As has already been

Table IV. Relative error in particle-momentum measurements $(\Delta p/p)_s$ and probable error Δ_{sign} in the determination of the particle sign in a propane chamber for track lengths of 5 cm and 25 cm, for particles of various mass

P, Mev/c	Track length = 5 cm						Track length = 25 cm					
	$M=1m_e$		$M=200m_e$		$M=2000m_e$		$M=1m_e$		$M=200m_e$		$M=2000m_e$	
	$(\Delta p/p)_s$	Δ_{sign}	$(\Delta p/p)_s$	Δ_{sign}	$(\Delta p/p)_s$	Δ_{sign}	$(\Delta p/p)_s$	Δ_{sign}	$(\Delta p/p)_s$	Δ_{sign}	$(\Delta p/p)_s$	Δ_{sign}
30	0,29	$<10^{-8}$		10^{-1}			0,13	10^{-9}	0,32	10^{-4}		
50	0,29	$<10^{-8}$	0,70	$<10^{-2}$			0,13	10^{-9}	0,30	10^{-8}		
70	0,29	$<10^{-8}$	0,52	$<10^{-4}$			0,13	10^{-9}	0,23	10^{-8}		
100	0,29	$<10^{-8}$	0,43	$<10^{-7}$			0,13	10^{-9}	0,19	10^{-8}		
200	0,29	$<10^{-8}$	0,36	$<10^{-8}$			0,13	10^{-9}	0,15	10^{-8}		
300	0,29	$<10^{-8}$	0,31	$<10^{-8}$	0,98	10^{-1}	0,13	10^{-9}	0,14	10^{-8}	0,45	10^{-4}
500	0,29	$<10^{-8}$	0,30	$<10^{-8}$	0,60	$<10^{-2}$	0,13	10^{-9}	0,13	10^{-8}	0,26	10^{-6}
1000	0,29	$<10^{-8}$	0,30	$<10^{-8}$	0,42	$<10^{-4}$	0,13	10^{-9}	0,13	10^{-8}	0,19	10^{-8}

mentioned, local distortions of the particle tracks in well-designed bubble chambers are small, and the particle track consists of very sharp bubble images.* It is therefore plausible that the multiple scattering of particles in the liquid can be used successfully for making measurements. In fact, the investigations[53-55] of photographs taken in propane bubble chambers have shown that such measurements lead in many cases to useful results. While measurements according to the angular method have been made in some experiments,[53] the more effective method of second differences has been used in other experiments.[54,55] Second differences were calculated using the distances of a track from a straight reference line, measured at the ends of cells chosen for the measurement. The optimum conditions for carrying out such measurements have been investigated in detail in reference 54.

As is well known,[56] the mean projected scattering angle is given by the equation

$$\bar{\Phi} = \frac{D_t}{t} = \frac{KZt^{1/2}}{p\beta c}, \qquad (32)$$

where Z is the particle charge, t the thickness of the scattering layer (cell length), K the scattering constant of the substance, and $\bar{D}_t$ the mean second difference over the cell length.

The value of the scattering constant K is determined by the composition of the scattering substance, and can either be calculated from the formulas of Williams[57] or Moliere,[58] or determined from experimental data on the scattering of particles with a given energy (see, e.g., reference 54).

Equation (32) was obtained under the assumption that the plane in which the projection of the scattering angle is measured passes through the original direction of the track. In practice, it is convenient to measure the deflections in the plane of the film. In those cases where the particle track in the chamber does not lie in a plane parallel to the film plane, it is necessary to introduce a correction for the inclination of the particle track with respect to the film plane, as is done in measurements with nuclear emulsions.[59] If θ_i is the angle of dip of the track with respect to the film plane, then,

$$p\beta c = Ks^{3/2} \sec \theta_i^{3/2} \bar{D}^{-1}. \qquad (33)$$

The mean second difference for a scattered particle is calculated from the second differences at the ends of the cells, according to the formula

$$\bar{D}_t = \sqrt{\bar{D}^2_{meas} - \bar{D}^2_{noise}}, \qquad (34)$$

where $\bar{D}_{noise}$ is the mean second difference due to apparent scattering (noise), observed along a particle track under given measurement conditions.

*The distortion of the tracks due to optical factors and other causes is not important in multiple-scattering measurements. Where other systematic distortions exist, the method of scattering measurements is similar to that used in measurements with nuclear emulsions when taking emulsion shrinkage into account.

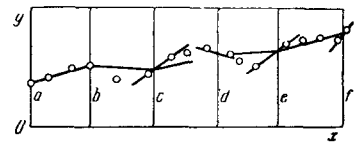

FIG. 9. Method of measuring the deflection of particle tracks at the ends of a cell. The circles correspond to bubble images. If a bubble is absent at the end of a cell, the deflection of the track is measured according to the line passing through the centers of two or three adjacent bubbles.

The method of measuring the deflections of the particle track is shown in Fig. 9. A more-detailed description of the measurement procedure is given in reference 54. We shall, however, mention some more important details. A successful multiple-scattering measurement is possible only with particle-track photography of good quality. It is necessary that the tracks consist of small bubbles. In that case, the interference of bubbles is practically negligible, and errors in measuring the coordinates of the bubble-image centers are avoided. Furthermore, it is necessary that the bubble density along the track be as high as possible. Given a sufficiently high bubble density, it is possible to carry out deflection measurements of the "smoothed-out" track at the ends of the cells, thus excluding random fluctuations in the bubble position. In such a case, the noise along the particle tracks decreases. In calculating second differences, it is necessary to take the fact that the cell length is measured on the film into account, and the deflection at the end of the cell should be corrected by a factor accounting for the difference in the magnification in photographing tracks located at different depths of the chamber.

The value of K for propane (the density of the technical propane used was 0.42 g/cm^3) from measurements on μ-meson tracks with a known energy is 4.3 ± 0.3 Mev-deg/100 μm, which is in good agreement with the calculated value.[57,58]

In measuring the momentum of sufficiently fast particles on track segments not very close to the end

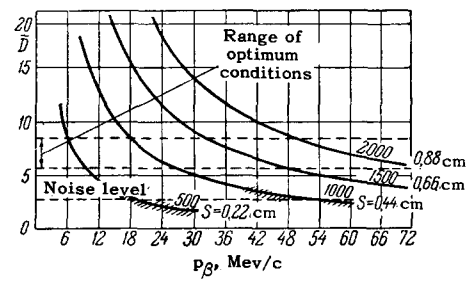

FIG. 10. Graphs for choosing the cell length for multiple-scattering measurements in propane bubble chambers. The cell length should correspond to the optimum region. The x axis represents the expected values of particle momentum in Mev/c, and the y axis the quantity $\bar{D}$ in the divisions of the microscope ocular which was used to measure the deflection of the bubble-image centers. One division of the micrometer equals a segment of 12.4×10^{-4} cm in the chamber.

Table V. Comparative characteristics of various working liquids of bubble chambers and of nuclear emulsions

Liquid	Liquid density in working conditions g/cm³	Stopping power compared with Al	Nuclear interaction mean free path, cm	Multiple-scattering coefficient
Propane. . .	0.43	0.22	97	1.06
Xenon. . . .	2.3	0.62	63	7.15
WF_6	2.4	0.72	42	6.94
$SnCl_4$	1.4	0.44	77	4.43
Nuclear emulsion .	3.8	0.98	26	7.64

of the track, we can divide the tracks into cells of equal length. The cell length is chosen so as to minimize the statistical error of the measurements (see graphs in Fig. 10, taken from reference 54). In measuring the momentum of particles of ~ 100 Mev/c in a propane bubble chamber, the cell length should equal 0.88 cm. In that case, for a track length equal to 10 cm, the value of $p\beta c$ will be obtained with a statistical error of ~ 25%.

Conditions for measuring $p\beta c$ are much better in chambers filled with high-Z liquids [(see Eq. (30)]. A comparison of different liquids and of the ratio of their scattering properties can be made with the help of Table V, compiled from the data of reference 26.

In order to find the particle mass, it is necessary to measure two independent parameters. Thus, if we use the values of $p\beta c$ determined from multiple-scattering measurements, then, in order to find the mass, it is also necessary to measure the ionization or range of the particle. Ionization-scattering relations are used for measuring the mass of particles which do not stop in the chamber. For particles stopping in the chamber, the mass should be determined from measurements of the momentum and of the residual range (see reference 50). This method of particle-mass measurement in propane chambers[54,55] (using groups of tracks of known particles) has led to a good agreement between the measured and real values of the mass of these particles.

5.2. MEASUREMENTS USING THE VARIABLE-CELL METHOD

Results of multiple-scattering measurements on particle tracks in bubble chambers using the variable-cell method developed for nuclear emulsions[60-62] are reported in reference 55. The variable-cell method ensures an improved statistical accuracy of the results because of the increased number of cells used for the measurement, and also reduces the error introduced by the not-fully correct exclusion of "very large" deflections. Measurements using this method are especially effective if the track of the investigated particle stops in the chamber, and is of considerable length. In that case, we can determine the π-meson mass with an error of 25% from measurements on a single track, and can thus separate well the tracks of π mesons, K mesons, and protons stopping in the chamber. A calculation of the cell length which should be used for the measurements of second differences in determining the particle mass in a propane bubble chamber has been presented.[55] It was found[55] that, in measuring the scattering on tracks of good quality, we can use a cell length corresponding to twice the natural scattering due to noise.

The statistical error of the particle-mass measurements in a propane chamber is, to a first approximation, given by the formula

$$\frac{dM'}{M'} \sim \frac{1,9}{\sqrt{n}}, \tag{35}$$

where M is the particle mass, and n is the number of cells used in the measurement.

From the above, it is obvious that the multiple-scattering measurements on particle tracks in bubble chambers filled with heavy liquids can be very useful for the identification of particles. It should, however, be mentioned that it is necessary to exercise great care in the visual estimates of multiple scattering. Very often, an apparently curved track is not due to multiple scattering, but rather to three or four single Coulomb-scattering events. Upon a more exact investigation, such a track is found to be not an arc, but rather a series of straight segments. This fact should be taken into account in using the multiple-scattering method for qualitative estimates.

5.3. Particle-Momentum Determination from Measurements of the Track Curvature due to the Combined Action of the Magnetic Field and Multiple Scattering

The analysis of particle tracks produced under the combined action of the magnetic field and the Coulomb scattering field has been discussed by a number of authors.[52,63,64]

The problem is especially important for bubble chambers. Because of the considerable dimensions of the bubble chambers, the magnets used with these instruments can only possess an intensity of 20 to 30 kilogauss, i.e., by one order of magnitude less than the intensities attainable in emulsion work. On the other hand, for the majority of the liquids used, multiple scattering attains a considerable magnitude. The particle tracks to be analyzed are therefore produced under conditions for which neither the Coulomb nor the magnetic field is by itself predominating, i.e., neither one of the two factors can be considered predominant as compared with the other. In such a case, the curvature of the track due to multiple scattering considerably adds to the information concerning the particle momentum obtained from an interpretation of the experimental data based only on the magnetic deflection. On the other hand, if the charge of the par-

ticle is known, any magnetic deflection, even a small one, can considerably add to the information on the particle momentum obtained from the scattering data for a zero magnetic field. Thus, e.g.,[64] for a 1 cm long track of a very fast particle in nuclear emulsion, the information on the momentum obtained in a magnetic field of 300 000 gauss and taking the multiple scattering into account is equivalent to the information obtained by measuring the particle momentum on a track 9.2 cm long at zero magnetic field. Under the same conditions, but interpreting the experimental data without taking the scattering into account, the information obtained corresponds to an effective track length of 8.2 cm at zero magnetic field. Thus, under these conditions, the contribution to the information made by taking the scattering into account is small. However, for a magnetic field of 100 000 gauss, the contribution made to the information on the momentum by taking multiple scattering into account is equivalent to an increase of the effective track length by a factor of 2.3.

Equations for determining the most-probable value of the particle momentum, the projected root-mean-square angle of scattering $\theta_s = KL^{1/2} \mid Z \mid p\beta$, and the angle of particle deflection in the magnetic field

$$\theta_m = \frac{HLZ}{pc}$$

are given in reference 64.

If w_n is one of the N angles between the consecutive tangents to the track at equal intervals L, and θ_e is the root-mean-square deflection due to the noise, then the most probable values of θ_s and θ_m corresponding to the measured values of w_n are given by the relation

$$\frac{1}{N}\sum_{n=1}^{N} w_n^2 - \theta_s^2 - \theta_e^2 - \theta_m \frac{1}{N}\sum_{n=1}^{N} w_n + \frac{\theta_e^2}{\theta_s^2}\theta_m\left(\frac{1}{N}\sum_{n=1}^{N} w_n - \theta_m\right) = 0. \quad (36)$$

In the limiting cases of a strong magnetic field on one hand, or of large scattering on the other, we can obtain approximate expressions for θ_m or θ_s from Eq. (36).

Under experimental conditions, the best estimates of θ_m and θ_s for fixed values of θ_m/θ_s and θ_e can be obtained by a graphical method, corresponding to Eq. (36).

An analysis of the optimum conditions with respect to the magnitude of the magnetic field and of the multiple scattering, which must be fulfilled for the most effective estimate of the particle mass and for the determination of the sign of its charge, has also been carried out.[64]

6. PROBLEMS CONNECTED WITH THE BUBBLE-CHAMBER METHOD

The rapid development of the bubble-chamber technique and of devices for the automatic evaluation of particle-track photographs is due to the suitability of bubble chambers for work with high-energy particle accelerators.

Increasing the dimensions of the chamber not only increases the detection efficiency of rare events, but also increases the measurement accuracy. New possibilities for measuring a number of physical processes arise. Thus, for example, in chambers having sufficiently large dimensions, it is possible to carry out statistical measurements of the lifetime of unstable particles, using the method developed for cloud chambers.[65,66,67] Using chambers filled with heavy liquids, a direct measurement of the characteristics of γ emission, of cascade processes, etc. becomes possible.

The great amount of information contained in the hundreds of thousands of particle-track photographs taken in bubble chambers operating with accelerators makes it important to concentrate efforts on the development of automatic devices for the scanning and evaluation of particle tracks.

Efforts to produce devices for the automatic (or semi-automatic) measurement of the coordinates of particle-track points, and for a presentation of the data in a form suitable for electronic computers, have met with considerable success.[70,73] Subjective errors due to parallax in making the coordinate measurements are eliminated in these devices. It is also no longer necessary to carry out the tedious and difficult work of computing the real coordinates of the particle tracks, of checking the complanarity of the tracks, of calculating the track curvature, etc.

However, interesting events are, as a rule, only contained in a small fraction of the bubble-chamber photographs. These events must be searched for by observers through visual scanning of stereoscopic photographs of the particle tracks. The scanning of the pictures involves a considerable amount of work, and may in itself lead to errors in the interpretation of the results obtained because of a subjective bias in the selection of events. Effective programs for the automatization of the scanning process have not as yet been worked out, but the general progress in the field of automatization makes it possible to hope for results in this field also.

Recently, chambers have been built with scintillators added in the working liquid.[74] Such chambers, operated with coincidence and anticoincidence circuits of scintillation counters, avoid the loss of time and the expense involved in taking and evaluating photographs which do not contain events of special interest.

[1] D. A. Glaser, Phys. Rev. **87**, 665 (1952).

[2] D. A. Glaser, Phys. Rev. **91** (1953).

[3] R. H. Hildebrand and D. E. Nagle, Phys. Rev. **92**, 517 (1953).

[4] I. G. Wood, Phys. Rev. **94**, 731 (1954).

[5] L. W. Alvarez, CERN Symposium **2**, 13 (1956).

[6] Kolganov, Lebedev, Nikitin, and Smolyankin, Приборы и техника эксперимента (Instruments and Exptl. Technique) No. 1 (1958).

[7] Blinov, Krestnikov, and Pershin, Doklady Akad. Nauk SSSR **99**, 929 (1954); Izv. Akad. Nauk SSSR Ser. Fiz. **19**, 758 (1955), Columbia Tech. Transl. p. 685.

[8] I. I. Pershin, op. cit. ref. 6, No. 1, 39 (1957).

[9] Blinov, Krestnikov, and Lomanov, JETP **31**, 762 (1956), Soviet Phys. JETP **4**, 661 (1957).

[10] Kolganov, Lebedev, Nikitin, Smolyankin, and Sokolov, op. cit. ref. 6, No. 4, 30 (1958).

[11] Brown, Glaser, and Perl, Phys. Rev. **102**, 586 (1956); Brown, Dodd, Glaser, and Perl, CERN Symposium **2**, 3 (1956).

[12] Fairbank, Harth, Blevins, and Slaughter, Phys. Rev. **100**, 971 (1955).

[13] Argan, Conte, Gigli, Picasso, and Gonella, Nuovo cimento **10**, 182 (1958).

[14] R. I. Plano and I. A. Pless, Phys. Rev. **99**, 639 (1955) (pentane bubble chamber).

[15] B. Hahn and G. Riepe, Rev. Sci. Instr. **29**, 184 (1958) (bubble chamber with fluorocarbon compounds).

[16] E. V. Kuznetsov and I. Ya. Timoshin, op. cit. ref. 6, No. 4, 40 (1959) (xenon bubble chamber).

[17] Wang, Solov'ev, and Shkobin, op. cit. ref. 6, No. 1, 41 (1959) (propane bubble chamber).

[18] I. D. Cow and A. H. Rosenfeld, Proceedings of the International Conference on High-Energy Accelerators and Instrumentation, CERN, 1959, p. 435 (large bubble chamber).

[19] Bloch, Lagarrigue, Musset, Rancon, Rousset, Sauteron, and Six, ibid., p. 499 (large bubble chamber with heavy liquids).

[20] W. M. Powell, ibid., p. 493.

[21] C. Dodd, Progr. Nucl. Phys., London **5**, 142 (1959).

[22] H. Slätis, Nucl. Instruments **7**, 1 (1959).

[23] D. A. Glaser, Handb. Phys. (Springer-Verlag, Berlin, 1958) Vol. 45 (II), p. 314.

[24] E. V. Kuznetsov, Usp. Fiz. Nauk **64**, 34 (1958).

[25] Blinov, Pomanov, Meshkovskii, Shalamov, and Shebanov, op. cit. ref. 6, No. 1, 35 (1958) (bubble chamber with fluorine mixture).

[26] Alyea, Gallagher, Mullnis, and Teem, Nuovo cimento **6**, 1480 (1957) (bubble chamber with WF_6).

[27] Bullock, Dodd, and Kolmus, Nuovo cimento **10**, 718 (1958) (bubble chamber filled with methyliodide-propane and $CBrF_3$).

[28] Alikhan'yan, Veremeev, Gal'per, Kirillov-Ugryumov, Kotenko, Kuzin, Kuznetsov, and Popov, Proceedings of the International Conference on High-Energy Accelerators and Instrumentation, CERN, 1959 (570-liter bubble chamber with freon mixture).

[29] Ya. Ya. Shalamov and V. A. Shebanov, ibid., p. 512 (bubble chamber with xenon-propane and freon-propane mixtures).

[30] Bertanza, Franzini, Mannelli, and Silvestrini, Nuovo cimento **10**, 403 (1958).

[31] Hahn, Riepe, and Knudsen, Rev. Sci. Instr. **30**, 654 (1959).

[32] High-Energy Particle Data, vol. II, ed. Y. H. Atkinson and B. H. Willis, Radiation Laboratory Berkeley, California, 1957.

[33] Aleksandrov, Gorbunkov, Delone, and Likhachev, op. cit. ref. 6, No. 1, 113 (1960).

[34] P. M. S. Blackett, Nuovo cimento **11**, Supplemento, 264 (1954).

[35] Budde, Burger, Filtuth, Goldschmidt-Clermont, Mayer, Morrison, Peyrou, and Trembley, Nuovo cimento **14**, 778 (1959).

[36] M. Cresti, UCRL Engg. Note, 4312-07 (M-37 and M-37b).

[37] Evans, Hadley, Morgan, Williams, and Kirk, J. Sci. Instr. **36**, 365 (1959).

[38] Bassi, Loria, Meyer, Mittner, and Scotoni, Nuovo cimento **5**, 1729 (1957).

[39] Borelli, Franzini, Mannelli, Minguzi-Ranzi, Santangelo, Saporetti, Silvestrini, Waloschek, and Zoboli, Nuovo cimento **3**, 525 (1958).

[40] Barmin, Kanavets, Morozov, and Pershin, JETP **34**, 830 (1958), Soviet Phys. JETP **7**, 573 (1959).

[41] Alikhan'yan, Kirillov-Ugryumov, Kotenko, Kuznetsov, and Popov, JETP **34**, 1101 (1958), Soviet Phys. JETP **7**, 763 (1958).

[42] Balandin, Moiseenko, Mukhin, and Otvinovskii, JETP **36**, 424 (1959), Soviet Phys. JETP **9**, 296 (1959).

[43] Bertanza, Martelli, and Tallini, Nuovo cimento **5**, Suppl. No. 4, 940 (1957).

[44] G. A. Askar'yan, JETP **30**, 610 (1956), Soviet Phys. JETP **3**, 640 (1956).

[45] Hahn, Knudsen, and Hugentobler, Nuovo cimento **15**, Suppl. No. 2, 236 (1960).

[46] M. F. Pomanov and B. V. Chirikov, op. cit. ref. 6, No. 5, 22 (1957).

[47] Glaser, Rahm, and Dodd, Phys. Rev. **102**, 1653 (1956).

[48] Willis, Fowler, and Rahm, Phys. Rev. **108**, 1046 (1957).

[49] L. Derado and H. Schmitz, Nuovo cimento **11**, Suppl. No. 6, 887 (1959).

[50] B. Rossi, High-Energy Particles, Prentice Hall, New York, 1952.

[51] E. H. S. Burhop, Nuovo cimento **2**, Supplemento, 343 (1954).

[52] I. E. Moyal, Phil. Mag. **41**, 1059 (1950).

[53] Kirillov-Ugryumov, Kotenko, Kuxnetsov, and Samoĭlov, op. cit. ref. 6, No. 1, 44 (1958).

[54] Pershin, Barmin, Kanavets, and Morozov, op. cit. ref. 6, No. 4, 44 (1959).

[55] I. I. Pershin and V. M. Golubchikov, op. cit. ref. 6, No. 3, 26 (1960).

[56] Gottstein, Menon, Mulvey, O'Ceallaigh, and Rochat, Phil. Mag. **42**, 708 (1951).

[57] E. I. Williams, Phys. Rev. **58**, 292 (1940).

[58] G. Moliere, Z. Naturforsch. **2a**, 133 (1947); **3a**, 78 (1948).

[59] M. G. K. Menon and C. O'Ceallaigh, Phil. Mag. **44**, 1291 (1953).

[60] Biswas, George, and Peters, Proc. Indian Acad. Sci. **38**, 413 (1953).

[61] Dilworth, Goldsack, and Hirschberg, Nuovo cimento **11**, 113 (1954).

[62] B. Roederer, Nuovo cimento **11**, Suppl. No. 1, 135 (1955).
[63] Groetzinger, Berger, and Ribe, Phys. Rev. **77**, 584 (1950).
[64] H. P. Furth, Rev. Sci. Instr. **26**, 1097 (1955).
[65] M. S. Bartlett, Phil. Mag. **44**, 249 (1953).
[66] W. B. Fretter and E. W. Friesen, Phys. Rev. **92**, 1089 (1953).
[67] I. G. Wilson and C. C. Butler, Phil. Mag. **43**, 993 (1952).
[68] Goldschmidt-Clermont, Van Dardell, Kowarski, and Peyrou, Nucl. Instr. **2**, 146 (1958).
[69] Van Dardell, Goldschmidt-Clermont, and Iselin, Nucl. Instr. **2**, 154 (1958).
[70] Y. Goldschmidt-Clermont, Proceedings of the International Conference on High-Energy Accelerators and Instrumentation, CERN, 1959, p. 523.
[71] Kaftanov, Lichtenbaum, Moiseev, Nikitin, and Fedotov, ibid., p. 550.
[72] Filippov, Kulyukin, Sherbakov, Sulyaev, and Vasilenko, ibid., p. 544.
[73] Andreev, Girsl, Zarubin, Kodykov, Korenchenko, Ladunov, Morozov, Nerkasov, Pose, Popov, Smirnov, and Tolstoy, ibid., p. 541.
[74] K. Strauch, ibid., p. 505.

Translated by H. Kasha